Journal of Solid Mechanics Vol. 15, No. 3 (2023) pp. 312-326
DOI: 10.22034/jsm.2023.1977290.1763

Research Paper

Vibration and Stability Analysis of Composite Tube Conveying Fluid Flow Equipped with Piezoelectric Ring

M. Nazarzadeh Ansarodi [1], H. Biglari [1], M.R. Saviz [2,*]

[1]*Mechanical Engineering Faculty, Tabriz University, Tabriz, Iran*
[2]*Mechanical Engineering Department, Azarbaijan Shahid Madani University, Tabriz, Iran*

Received 5 June 2023; accepted 4 August 2023

ABSTRACT

In this paper, dynamic behaviour of composite tube equipped with piezoelectric actuator ring and conveying fluid flow is studied. The effects of incompressible Newtonian internal fluid flow with constant velocity are considered. The stiffened composite shell with different boundary conditions is exposed to electro- mechanical loading. The governing equations of motion are obtained based on the classical shell theory and using Hamilton's principle. Then, these equations are discretized by using differential quadrature (DQ) method in longitudinal direction and harmonic differential quadrature (HDQ) method in circumferential direction. Solving these equations results in eigenvalues and mode shapes of the smart pipe conveying fluid. After comparing results with those existing in the literature, the detailed parametric study is conducted, by concentrating on the effects of fluid flow properties, geometry, material and boundary conditions of composite pipe, temperature, and piezo-actuator ring (size and position) on the vibration behavior of the coupled system, as well as dimensionless critical fluid velocity. It is expected that stability of the coupled system strongly depends on the imposed electric load. The present study can be applied for optimum design of sensors and actuators in active control systems, MEMS and biomechanical applications.

© 2023 IAU, Arak Branch.All rights reserved.

Keywords : Composite pipe; Piezoelectric ring; Instability; Critical fluid velocity; Differential quadrature method.

1 INTRODUCTION

SMART composite tubes have increasingly been used for transferring fluids in fuel and gas injectors, ink jet printer industries and even in medical applications, like artificial veins. Furthermore, cylindrical shells containing fluid flow have a lot of use in industrial systems like airplane motor, nuclear reactors, heat exchangers, fuel pipes and vessels. So, studying dynamic response of cylindrical laminated shells conveying fluid is very important in designing smart tubes. In 1998 Faria and Almeida [1], studied dynamic and static response of

*Corresponding author.
E-mail address: saviz@azaruniv.ac.ir (M.R.Saviz)

© 2023 IAU, Arak Branch. All rights reserved.

composite cylindrical shells equipped with piezoelectric ring. They solved equations of motion using finite element method and showed that piezo-actuators can have determining effects on static deformation and frequencies of pipes. In 2003 Zhang, Gorman and Reese [2] studied vibrations of cylindrical shell with Sanders theory and solved equations of motion with finite element method and studied the effects of internal pressure, fluid velocity and geometry of shell on vibrations of tubes. In 2004 Civalek [3] studied Application of Differential quadrature method and harmonic differential quadrature method for buckling analysis of thin isotropic plates and showed that harmonic differential quadrature method is more accurate than differential quadrature method. In 2004, Reddy and Wang [4] investigated dynamic response of fluid conveying pipes by using imaginary displacement method considering nonlinear terms with Euler Bernoulli and Timoshenko beam. They solved equations of motion with finite element method. Dynamic behaviour of laminated composite cylindrical shells has been studied by Saviz et al. [5], using layerwise shell theory for a layered composite cylindrical shell with piezoelectric rings. In 2010, Karagiozis, Amabili and Paidoussis[6] studied dynamic response of harmonically excited circular cylindrical shells containing fluid flow with considering nonlinear terms for clamped- simple boundary conditions and showed that vibrations of shell could be periodic or chaotic depending on velocity of fluid and frequency of excitation. In 2011, Bochkarev and Matveenko [7] studied natural vibrations of shells containing fluid flow using classic shell theory and solved equations of motion with finite element method for different boundary conditions and concluded that boundary conditions have large effect on natural frequency also thy showed that increasing length of pipe, decreases natural frequency. In 2012, Jannesari, Emami and Karimpour [8] studied effects of fluid viscosity on instability of carbon nanotubes containing fluid with nonlinear Donnell's theory and concluded that effect of viscosity depends on tubes diameter and that it can't be neglected for every diameter. In 2014 Ke, Wang and Reddy [9] studied thermo electro mechanical vibration of cylindrical Nano shells under various boundary conditions by using Lave theory. They solved equations of motion with differential quadrature method for different boundary conditions and studied effects of temperature, voltage, radius to thickness ratio and length to radius ratio on natural frequency. In 2016, Maalawi et. Al. [10] studied and designed composite pipes conveying fluid to improved stability characteristics and showed that geometric parameters have great influences on instability of tubes.

In this paper, dynamic behavior of composite tube with incompressible Newtonian fluid flow is studied. There are few papers in which the tube is considered to be a Piezo-Composite. However, for the first time, the composite pipe with internal flow and stiffened with piezoelectric actuator rings is under investigation. The classical shell theory (Love-Kirchhoff hypothesis) is used for modeling kinematics of thin composite shell and the equations of motion are obtained using Hamilton's principle. Then, these equations are discretized by using differential quadrature (DQ) method in axial direction and harmonic differential quadrature (HDQ) method in peripheral direction. The resulting equations are used to calculate the eigenvalues and eigenvectors of fluid conveying smart pipes. After making verifications about the accuracy of some results, the effects of different parameters of fluid flow (viscosity, density and velocity), composite tube (geometry, number and orientation of layers and boundary conditions), and piezo-actuator ring (length and place of ring, and applied voltage) on shell natural frequency and dimensionless critical fluid velocity are studied.

2 FORMULATION

A schematic configuration of pipe and polar coordinate system is shown in Fig. 1. Based on the classical shell theory, the displacement field can be expressed as:

$$\begin{aligned} u_1(x,\theta,z,t) &= u(x,\theta,t) - z\frac{\partial w}{\partial x} \\ v_1(x,\theta,z,t) &= v(x,\theta,t) - z\frac{\partial w}{\partial \theta} \\ w_1(x,\theta,z,t) &= w(x,\theta,t) \end{aligned} \tag{1}$$

where u_1, v_1, w_1 denote the displacement of an arbitrary point of tube and u, v and w are displacements of mid-plane of tube (z=0).

© 2023 IAU, Arak Branch

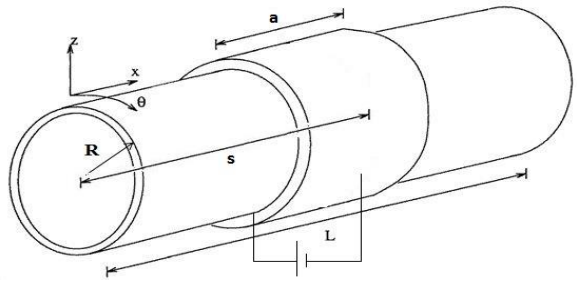

Fig.1
Configuration of composite pipe equipped with piezoelectric ring actuator.

The linear von karman strain field could be expressed in the following form:

$$\begin{aligned}
&\varepsilon_{xx} = \varepsilon_x^0 + z\,\varepsilon_x^1 \\
&\varepsilon_{\theta\theta} = \varepsilon_\theta^0 + z\,\varepsilon_\theta^1 \\
&\gamma_{x\theta}^0 = \varepsilon_{x\theta m} + z\,\gamma_{x\theta}^1
\end{aligned} \tag{2}$$

In which,

$$\begin{Bmatrix} \varepsilon_x^0 + z\,\varepsilon_x^1 \\ \varepsilon_\theta^0 + z\,\varepsilon_\theta^1 \\ \gamma_{x\theta}^0 + z\,\gamma_{x\theta}^1 \end{Bmatrix} = \begin{Bmatrix} \dfrac{\partial u}{\partial x} \\ \dfrac{\partial v}{R\,\partial\theta} + \dfrac{w}{R} \\ \dfrac{\partial u}{R\,\partial\theta} + \dfrac{\partial v}{\partial x} \end{Bmatrix} - z \begin{Bmatrix} \dfrac{\partial^2 w}{\partial x^2} \\ \dfrac{\partial^2 w}{R^2\partial\theta^2} \\ 2\dfrac{\partial^2 w}{R\,\partial x\,\partial\theta} \end{Bmatrix} \tag{3}$$

The piezo-ring is considered only as actuator, so that, there is a one way coupling between elastic and electrical fields as well as thermal field. The constitutive equations for stresses and strains in the presence of thermal and electrical field could be written as, [11]

$$\begin{Bmatrix} \sigma_x \\ \sigma_\theta \\ \sigma_{x\theta} \end{Bmatrix}^{(k)} = \begin{bmatrix} Q_{11} & Q_{12} & 0 \\ Q_{12} & Q_{22} & 0 \\ 0 & 0 & Q_{66} \end{bmatrix}^{(k)} \begin{Bmatrix} \varepsilon_x - \alpha_1\Delta T \\ \varepsilon_\theta - \alpha_2\Delta T \\ \gamma_{x\theta} \end{Bmatrix} - \begin{bmatrix} 0 & 0 & e_{31} \\ 0 & 0 & e_{32} \\ 0 & 0 & 0 \end{bmatrix}^{(k)} \begin{Bmatrix} E_x \\ E_\theta \\ E_{x\theta} \end{Bmatrix}^{(k)} \tag{4}$$

where e_{ij} are the piezoelectric constants and Q_{ij} are the elastic constants of k_{th} layer, given as follows:

$$Q_{11} = \frac{E_1}{1-\nu_{12}\nu_{21}}, Q_{12} = \frac{\nu_{12}E_2}{1-\nu_{12}\nu_{21}}, Q_{21} = \frac{\nu_{21}E_1}{1-\nu_{12}\nu_{21}}, Q_{22} = \frac{E_2}{1-\nu_{12}\nu_{21}}, Q_{66} = G_{12} \tag{5}$$

Stress resultant- strain relations can be written as:

$$\begin{Bmatrix} N_{xx} \\ N_{\theta\theta} \\ N_{x\theta} \end{Bmatrix} = \begin{bmatrix} A_{11} & A_{12} & A_{16} \\ A_{12} & A_{22} & A_{26} \\ A_{16} & A_{26} & A_{66} \end{bmatrix} \begin{Bmatrix} \varepsilon_{xx} \\ \varepsilon_{\theta\theta} \\ \gamma_{x\theta} \end{Bmatrix}^{(0)} + \begin{bmatrix} B_{11} & B_{12} & B_{16} \\ B_{12} & B_{22} & B_{26} \\ B_{16} & B_{26} & B_{66} \end{bmatrix} \begin{Bmatrix} \varepsilon_{xx} \\ \varepsilon_{\theta\theta} \\ \gamma_{x\theta} \end{Bmatrix}^{(1)} - \begin{Bmatrix} N_{xx} \\ N_{\theta\theta} \\ N_{x\theta} \end{Bmatrix}^{(p)} - \begin{Bmatrix} N_{xx} \\ N_{\theta\theta} \\ N_{x\theta} \end{Bmatrix}^{(T)} \tag{6}$$

$$\begin{Bmatrix} M_{xx} \\ M_{\theta\theta} \\ M_{x\theta} \end{Bmatrix} = \begin{bmatrix} B_{11} & B_{12} & B_{16} \\ B_{12} & B_{22} & B_{26} \\ B_{16} & B_{26} & B_{66} \end{bmatrix} \begin{Bmatrix} \varepsilon_{xx} \\ \varepsilon_{\theta\theta} \\ \gamma_{x\theta} \end{Bmatrix}^{(0)} + \begin{bmatrix} D_{11} & D_{12} & D_{16} \\ D_{12} & D_{22} & D_{26} \\ D_{16} & D_{26} & D_{66} \end{bmatrix} \begin{Bmatrix} \varepsilon_{xx} \\ \varepsilon_{\theta\theta} \\ \gamma_{x\theta} \end{Bmatrix}^{(1)} - \begin{Bmatrix} M_{xx} \\ M_{\theta\theta} \\ M_{x\theta} \end{Bmatrix}^{(p)} - \begin{Bmatrix} M_{xx} \\ M_{\theta\theta} \\ M_{x\theta} \end{Bmatrix}^{(T)} \tag{7}$$

© 2023 IAU, Arak Branch

Eqs. 6 and 7 can be written in matrix form as:

$$\begin{Bmatrix}\{N\}\\ \{M\}\end{Bmatrix}=\begin{bmatrix}[A] & [B]\\ [B] & [D]\end{bmatrix}\begin{Bmatrix}\{\varepsilon^0\}\\ \{\varepsilon^1\}\end{Bmatrix}-\begin{Bmatrix}\{N^T\}\\ \{M^T\}\end{Bmatrix}-\begin{Bmatrix}\{N^P\}\\ \{M^P\}\end{Bmatrix} \tag{8}$$

where, the components of sub-matrices are given as follows,

$$\begin{aligned}
A_{ij} &= \int_{-h/2}^{h/2}\bar{Q}_{ij}dz = \sum_{k=1}^{N}\left[\bar{Q}_{ij}\right]_k (z_{k+1}-z_k)\\
B_{ij} &= \int_{-h/2}^{h/2}\bar{Q}_{ij}zdz = \frac{1}{2}\sum_{k=1}^{N}\left[\bar{Q}_{ij}\right]_k (z_{k+1}^2-z_k^2)\\
D_{ij} &= \int_{-h/2}^{h/2}\bar{Q}_{ij}z^2dz = \frac{1}{3}\sum_{k=1}^{N}\left[\bar{Q}_{ij}\right]_k (z_{k+1}^3-z_k^3)\\
\left\{N_i^P\right\} &= \sum_{k=1}^{N}\int_{z_{k+1}}^{z_k}\left[\bar{Q}_{ij}\right]_k \{\bar{e}\}^k [E]^k Edz\\
\left\{M_i^P\right\} &= \sum_{k=1}^{N}\int_{z_{k+1}}^{z_k}\left[\bar{Q}_{ij}\right]_k \{\bar{e}\}^k [E]^k Ezdz
\end{aligned} \tag{9}$$

$$\begin{aligned}
\left\{N_{xx}^T\right\} &= \int_{-\frac{h}{2}}^{\frac{h}{2}}\{C_{11}(T)\alpha_{xx}+C_{12}(T)\alpha_{\theta\theta}\}\Delta Tdz\\
\left\{N_{\theta\theta}^T\right\} &= \int_{-\frac{h}{2}}^{\frac{h}{2}}\{C_{21}(T)\alpha_{xx}+C_{22}(T)\alpha_{\theta\theta}\}\Delta Tdz\\
\left\{M_{xx}^T\right\} &= \int_{-\frac{h}{2}}^{\frac{h}{2}}\{C_{11}(T)\alpha_{xx}+C_{12}(T)\alpha_{\theta\theta}\}\Delta Tzdz\\
\left\{M_{\theta\theta}^T\right\} &= \int_{-\frac{h}{2}}^{\frac{h}{2}}\{C_{21}(T)\alpha_{xx}+C_{22}(T)\alpha_{\theta\theta}\}\Delta Tzdz
\end{aligned} \tag{10}$$

3 ENERGY METHOD

The strain energy of the composite pipe can be written as [13]

$$U=\int_V\left(\sigma_x\varepsilon_x+\sigma_\theta\varepsilon_\theta+\sigma_{x\theta}\varepsilon_{x\theta}\right)dV \tag{11}$$

Combining Eq. (11) with strain- displacement relations (Eq. (3)) yields

$$U=\int_{-\frac{h}{2}}^{\frac{h}{2}}\int_A\left\{\sigma_x\left(\frac{\partial u}{\partial x}-z\frac{\partial^2 w}{\partial x^2}\right)+\sigma_\theta\left(\frac{\partial v}{R\partial\theta}+\frac{w}{R}-z\frac{\partial^2 w}{R^2\partial\theta^2}\right)+\sigma_{x\theta}\left(\frac{\partial u}{R\partial\theta}+\frac{\partial v}{\partial x}-2z\frac{\partial^2 w}{R\partial\theta\partial x}\right)\right\}dzdA \tag{12}$$

© 2023 IAU, Arak Branch

By integrating through thickness the potential energy is written as:

$$U=\int_{A}\left\{N_{xx}\left(\frac{\partial u}{\partial x}\right)-M_{xx}\frac{\partial^2 w}{\partial x^2}+N_{\theta\theta}\left(\frac{\partial v}{R\partial\theta}+\frac{w}{R}\right)-M_{\theta\theta}\frac{\partial^2 w}{R^2\partial\theta^2}+N_{x\theta}\left(\frac{\partial u}{R\partial\theta}+\frac{\partial v}{\partial x}\right)-2M_{x\theta}\frac{\partial^2 w}{R\partial\theta\partial x}\right\}dA \tag{13}$$

The kinetic energy of the pipe is written as, [13]

$$K=\frac{\rho}{2}\int_{V}\left(\left(\frac{\partial u}{\partial t}\right)^2+\left(\frac{\partial v}{\partial t}\right)^2+\left(\frac{\partial w}{\partial t}\right)^2\right)dV \tag{14}$$

Combining Eq. (14) with strain- displacement relations (Eq. (3)) yields

$$K=\frac{\rho}{2}\int_{-\frac{h}{2}}^{\frac{h}{2}}\int_{A}\left\{\left(\frac{\partial u}{\partial t}\right)^2-2z\frac{\partial u}{\partial t}\frac{\partial^2 w}{\partial t\partial x}+z^2\left(\frac{\partial^2 u}{\partial t\partial x}\right)^2+\left(\frac{\partial v}{\partial t}\right)^2-2z\frac{\partial v}{\partial t}\frac{\partial^2 w}{\partial t\partial x}+z^2\left(\frac{\partial^2 w}{\partial t\partial x}\right)^2+\left(\frac{\partial w}{\partial t}\right)^2\right\}dzdA \tag{15}$$

Strain energy of a typical piezoelectric actuator ring is as follows:

$$U=\int_{\frac{h}{2}}^{\frac{h}{2}+t_p}\int\left(\sigma_x\delta\varepsilon_x+\sigma_\theta\delta\varepsilon_\theta+\sigma_{x\theta}\delta\varepsilon_{x\theta}\right)\left[H\left(x-\left(s-\frac{a}{2}\right)\right)-H\left(x-\left(s+\frac{a}{2}\right)\right)\right]dzdA \tag{16}$$

Kinetic energy of piezoelectric ring is written as:

$$K=\int_{\frac{h}{2}}^{\frac{h}{2}+t_p}\int\rho_p\left[\dot{u}\delta\dot{u}+\dot{v}\delta\dot{v}+\dot{w}\delta\dot{w}\right]\left[H\left(x-\left(s-\frac{a}{2}\right)\right)-H\left(x-\left(s+\frac{a}{2}\right)\right)\right]dzdA \tag{17}$$

where, H is Heaviside function which is defined as:

$$H(x-a)=\begin{cases}1 & x\geq a\\ 0 & x<a\end{cases} \tag{18}$$

The constant electric field can be applied only in the radial direction to the ring.

4 EXTERNAL WORK DONE BY FLUID FLOW

By assuming the Newtonian fluid, the governing equation of the fluid can be described by the well-known Navier-Stokes equation as:

$$\rho\frac{d\vec{V}}{dt}=-\nabla P+\mu\nabla^2\vec{V}+F \tag{19a}$$

where $V=(v_x,v_\theta,v_z)$ is the flow velocity vector in cylindrical coordinate system with components in longitudinal x, circumferential θ and radial z directions. Also, P, μ and f ρ are the pressure, viscosity and density of the fluid, respectively and F_{body} denotes the body forces. In Navier-Stokes equation, the total derivative operator with respect to t is

© 2023 IAU, Arak Branch

$$\frac{d}{dt}=\frac{\partial}{\partial t}+v_x\frac{\partial}{\partial x}+v_\theta\frac{\partial}{R\partial\theta}+v_z\frac{\partial}{\partial z},$$
$$v_x=\frac{\partial u}{\partial t}+U_f\cos\theta \qquad v_x=\frac{\partial v}{\partial t} \qquad v_x=\frac{\partial w}{\partial t}-U_f\sin\theta \tag{19b}$$

U_f is the fluid velocity and u,v,w are displacements of mid-plane. By neglecting nonlinear terms, the components of the Navier-stocks equation can be written in terms of flow velocity and fluid mass m_f, [14]

$$\frac{\partial p}{\partial z}.A_f=-m_f\frac{\partial^2 w}{\partial t^2}-m_fU_f\frac{\partial^2 w}{\partial x\,\partial t}+\mu A_f\frac{\partial^3 w}{\partial x^2\partial t}-m_fU_f^2\frac{\partial^2 w}{\partial x^2}$$
$$+\mu A_f\frac{\partial^3 w}{\partial x^2\partial t}+U_f\mu A_f\frac{\partial^3 w}{\partial x^3}+\mu A_f\frac{1}{R^2}\frac{\partial^3 w}{\partial\theta^2\partial t}+\mu A_f\frac{U_f}{R^2}\frac{\partial^3 w}{\partial\theta^2\partial x} \tag{20}$$

$$\frac{\partial p}{\partial x}.A_f=-m_f\frac{\partial^2 v}{\partial t^2}-m_fU_f\frac{\partial^2 u}{\partial x\,\partial t}+\mu A_f\frac{\partial^3 u}{\partial x^2\partial t}+\mu A_f\frac{1}{R^2}\frac{\partial^3 u}{\partial\theta^2\partial t} \tag{21}$$

$$\frac{1}{R}\frac{\partial p}{\partial\theta}.A_f=-m_f\frac{\partial^2 v}{\partial t^2}-m_fU_f\frac{\partial^2 v}{\partial x\,\partial t}+\mu A_f\frac{\partial^3 v}{\partial x^2\partial t}+\mu A_f\frac{1}{R^2}\frac{\partial^3 v}{\partial\theta^2\partial t} \tag{22}$$

Finally, the external work due to the pressure of the fluid flow may be obtained as follows:

$$W=\int(F_{fluid})w\,dA$$

5 HAMILTON'S PRINCIPLE

Governing equations could be derived by using Hamilton's principal as follows:

$$\delta\int_0^t(K-U-V)dt=\int_0^t(\delta K-\delta U-\delta V)dt=0 \tag{23}$$

In which K, U and V were previously derived. Finally, the equations of motion are obtained as:

$$A_{11}\frac{\partial^2 u}{\partial x^2}+A_{12}\frac{\partial^2 v}{R\partial x\,\partial\theta}+A_{12}\frac{\partial w}{R\partial x}+A_{16}\frac{\partial^2 u}{R\partial x\,\partial\theta}+A_{16}\frac{\partial^2 v}{\partial x^2}+B_{11}\frac{\partial^3 w}{\partial x^3}+B_{12}\frac{\partial^3 w}{R^2\partial x\,\partial\theta^2}+2B_{16}\frac{\partial^3 w}{R\partial x^2\partial\theta}$$
$$-\frac{\partial N_{xx}^{p}}{\partial x}-\frac{\partial N_{xx}^{T}}{\partial x}+A_{16}\frac{\partial^2 u}{R\partial x\,\partial\theta}+A_{26}\frac{\partial^2 v}{R^2\partial\theta^2}+A_{26}\frac{\partial w}{R^2\partial\theta}+A_{66}\frac{\partial^2 u}{R^2\partial\theta^2}+A_{66}\frac{\partial^2 v}{R\partial x\,\partial\theta}+B_{16}\frac{\partial^3 w}{R\partial\theta\partial x^2}$$
$$+B_{26}\frac{\partial^3 w}{R^3\partial\theta^3}+2B_{66}\frac{\partial^3 w}{R^2\partial x\,\partial\theta^2}-\frac{1}{R}\frac{\partial N_{x\theta}^{p}}{\partial\theta}-\frac{1}{R}\frac{\partial N_{x\theta}^{T}}{\partial\theta}=I_0\ddot{u}-I_1\frac{\partial\ddot{w}}{\partial x}-m_f\frac{\partial^2 v}{\partial t^2}-m_fU_f\frac{\partial^2 u}{\partial x\,\partial t}$$
$$+\mu A_f\frac{\partial^3 u}{\partial x^2\partial t}+\mu A_f\frac{1}{R^2}\frac{\partial^3 u}{\partial\theta^2\partial t} \tag{24}$$

$$A_{12}\frac{\partial^2 u}{R\partial x\,\partial\theta}+A_{22}\frac{\partial^2 v}{R^2\partial\theta^2}+A_{22}\frac{\partial w}{R^2\partial\theta}+A_{26}\frac{\partial^2 u}{R^2\partial\theta^2}+A_{26}\frac{\partial^2 v}{R\partial x\,\partial\theta}+B_{12}\frac{\partial^3 w}{R\partial\theta\partial x^2}+B_{22}\frac{\partial^3 w}{R^3\partial\theta^3}+2B_{26}\frac{\partial^3 w}{R^2\partial x\,\partial\theta^2}$$
$$-\frac{1}{R}\frac{\partial N_{\theta\theta}^{p}}{\partial\theta}-\frac{1}{R}\frac{\partial N_{\theta\theta}^{T}}{\partial\theta}+A_{16}\frac{\partial^2 u}{\partial x^2}+A_{26}\frac{\partial^2 v}{R\partial x\,\partial\theta}+A_{26}\frac{\partial w}{R\partial x}+A_{66}\frac{\partial^2 u}{R\partial x\,\partial\theta}+A_{66}\frac{\partial^2 v}{\partial x^2}+B_{16}\frac{\partial^3 w}{\partial x^3}+B_{26}\frac{\partial^3 w}{R^2\partial x\,\partial\theta^2}$$
$$+2B_{66}\frac{\partial^3 w}{R\partial x^2\partial\theta}-\frac{\partial N_{x\theta}^{p}}{\partial x}-\frac{\partial N_{x\theta}^{T}}{\partial x}=I_0\ddot{v}-I_1\frac{\partial\ddot{w}}{\partial\theta}-m_f\frac{\partial^2 v}{\partial t^2}-m_fU_f\frac{\partial^2 v}{\partial x\,\partial t}+\mu A_f\frac{\partial^3 v}{\partial x^2\partial t}+\mu A_f\frac{1}{R^2}\frac{\partial^3 v}{\partial\theta^2\partial t} \tag{25}$$

© 2023 IAU, Arak Branch

$$
\begin{aligned}
&B_{11}\frac{\partial^3 u}{\partial x^3}+B_{12}\frac{\partial^3 v}{R\partial\theta\partial x^2}+B_{12}\frac{\partial^2 w}{R\partial x^2}+B_{16}\frac{\partial^3 u}{R\partial\theta\partial x^2}+B_{16}\frac{\partial^3 v}{\partial x^3}+D_{11}\frac{\partial^4 w}{\partial x^4}+D_{12}\frac{\partial^4 w}{R^2\partial x^2\partial\theta^2}+2D_{16}\frac{\partial^4 w}{R\partial x^3\partial\theta}\\
&-\frac{\partial^2 N_{xx}^{p}}{\partial x^2}-\frac{\partial^2 N_{xx}^{T}}{\partial x^2}-A_{12}\frac{\partial u}{R\partial x}-A_{22}\frac{\partial v}{R^2\partial\theta}-A_{22}\frac{w}{R^2}-A_{26}\frac{\partial u}{R^2\partial\theta}-A_{26}\frac{\partial v}{R\partial x}-B_{12}\frac{\partial^2 w}{R\partial x^2}-B_{22}\frac{\partial^2 w}{R^3\partial\theta^2}\\
&-2B_{26}\frac{\partial^2 w}{R^2\partial\theta\partial x}+\frac{N_{\theta\theta}^{p}}{R}+\frac{N_{\theta\theta}^{p}}{R}+B_{11}\frac{\partial^3 u}{R^2\partial\theta^2\partial x}+B_{12}\frac{\partial^3 v}{R^3\partial\theta^3}+B_{12}\frac{\partial^2 w}{R^3\partial\theta^2}+B_{16}\frac{\partial^3 u}{R^3\partial\theta^3}+B_{16}\frac{\partial^3 v}{R^2\partial\theta^2\partial x}\\
&+D_{11}\frac{\partial^4 w}{R^2\partial x^2\partial\theta^2}+D_{12}\frac{\partial^4 w}{R^4\partial\theta^4}+2D_{16}\frac{\partial^4 w}{R^3\partial x\partial\theta^3}-\frac{\partial^2 M_{xx}^{p}}{R^2\partial\theta^2}-\frac{\partial^2 M_{xx}^{T}}{R^2\partial\theta^2}+2B_{16}\frac{\partial^3 u}{R\partial x^2\partial\theta}+2B_{26}\frac{\partial^3 v}{R^2\partial x\partial\theta^2}\\
&+2B_{26}\frac{\partial^2 w}{R^2\partial x\partial\theta}+2B_{66}\frac{\partial^3 u}{R^2\partial x\partial\theta^2}+2B_{66}\frac{\partial^3 v}{R\partial x^2\partial\theta}+2D_{16}\frac{\partial^4 w}{R\partial x^3\partial\theta}+2D_{26}\frac{\partial^4 w}{R^3\partial x\partial\theta^3}+4D_{66}\frac{\partial^4 w}{R^2\partial x^2\partial\theta^2}\\
&-\frac{2\partial^2 M_{x\theta}^{p}}{R\partial x\partial\theta}-\frac{2\partial^2 M_{x\theta}^{T}}{R\partial x\partial\theta}=I_0\ddot{w}-I_2\frac{\partial^2\ddot{w}}{\partial x^2}-I_2\frac{\partial^2\ddot{w}}{\partial\theta^2}m_f\frac{\partial^2 w}{\partial t^2}-m_f U_f\frac{\partial^2 w}{\partial x\partial t}+\mu A_f\frac{\partial^3 w}{\partial x^2\partial t}-m_f U_f^2\frac{\partial^2 w}{\partial x^2}\\
&+\mu A_f\frac{\partial^3 w}{\partial x^2\partial t}+U_f\mu A_f\frac{\partial^3 w}{\partial x^3}+\mu A_f\frac{1}{R^2}\frac{\partial^3 w}{\partial\theta^2\partial t}+\mu A_f\frac{U_f}{R^2}\frac{\partial^3 w}{\partial\theta^2\partial x}
\end{aligned}
\tag{26}
$$

6 DIFFERNTIAL QUADRATURE METHOD

Numerical methods like finite element, Ritz, boundary element could have given accurate enough results, in case of taking sufficient number of mesh points into account. One of the numerical methods which deliver good results is differential quadrature method. Main relations of this method in two dimensional form are, [3]

$$
\frac{d^n f\left(x_i,\theta_j\right)}{dx^n}=\sum_{k=1}^{N_x}A_{ik}^{(n)}f\left(x_k,\theta_j\right)\qquad n=1,\ldots,N_x-1 \tag{27}
$$

$$
\frac{d^m f\left(x_i,\theta_j\right)}{d\theta^m}=\sum_{l=1}^{N_\theta}B_{jl}^{(m)}f\left(x_i,\theta_l\right)\qquad m=1,\ldots,N_\theta-1 \tag{28}
$$

$$
\frac{d^{n+m} f\left(x_i,\theta_j\right)}{dx^n d\theta^m}=\sum_{k=1}^{N_x}\sum_{l=1}^{N_\theta}A_{ik}^{(n)}B_{jl}^{(m)}f\left(x_k,\theta_l\right)\qquad m=1,\ldots,N_\theta-1\quad n=1,\ldots,N_x-1 \tag{29}
$$

where N_x and N_θ are the total number of spatial sampling points of the grid distribution in the axial and circumferential directions, respectively. A_{ik} and B_{jl} correspond to the weighting coefficients, which can be evaluated for the first and second order derivatives, as follows:

$$
A_{ij}^{(1)}=\begin{cases}\dfrac{M\left(x_i\right)}{\left(x_i-x_j\right)M\left(x_j\right)} & i,j=1,2,\ldots,N_x\quad\left(i\neq j\right)\\ -\displaystyle\sum_{j=1,i\neq j}^{N_x}A_{ij}^{(1)} & i,j=1,2,\ldots,N_x\quad\left(i=j\right)\end{cases} \tag{30}
$$

$$
B_{ij}^{(1)}=\begin{cases}\dfrac{P\left(\theta_i\right)}{\left(\theta_i-\theta_j\right)P\left(\theta_j\right)} & i,j=1,2,\ldots,N_\theta\quad\left(i\neq j\right)\\ -\displaystyle\sum_{j=1,i\neq j}^{N_\theta}B_{ij}^{(1)} & i,j=1,2,\ldots,N_\theta\quad\left(i=j\right)\end{cases} \tag{31}
$$

M and P are define as:

© 2023 IAU, Arak Branch

$$M(x_i) = \prod_{j=1, j\neq i}^{N_x} (x_i - x_j) \tag{32}$$

$$P(\theta_i) = \prod_{j=1, j\neq i}^{N_\theta} (\theta_i - \theta_j) \tag{33}$$

$$A_{ij}^{(n)} = n\left(A_{ii}^{(n-1)} A_{ij}^{(1)} - \frac{A_{ij}^{(n-1)}}{(x_i - x_j)}\right) \tag{34}$$

$$B_{ij}^{(m)} = m\left(B_{ii}^{(m-1)} B_{ij}^{(1)} - \frac{B_{ij}^{(m-1)}}{(\theta_i - \theta_j)}\right) \tag{35}$$

It is well known that the use of a grid distribution, which is denser on the boundaries, gives much better results in comparison with a uniform distribution in DQ analysis. Therefore, Chebyshev–Gauss–Labatto grid distribution is used to discretize the spatial coordinates as:

$$x_i = \frac{L}{2}\left[1 - \cos\left(\frac{i-1}{N_x - 1}\right)\pi\right] \qquad i = 1, \cdots, N_x$$

$$\theta_i = \frac{2\pi}{2}\left[1 - \cos\left(\frac{i-1}{N_\theta - 1}\right)\pi\right] \qquad i = 1, \cdots, N_\theta$$

The grid distribution is presented in Fig. 2

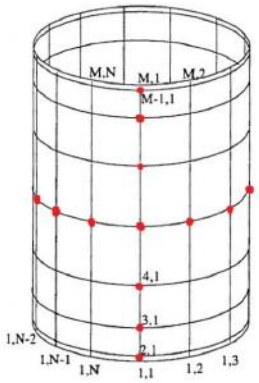

Fig.2
Chebyshev grid distribution for DQM.

By applying differential quadrature Eqs. (27-35) to Eqs. (24- 26), system of governing equations would emerge in the following matrix form

$$\begin{bmatrix} K_{bb} & K_{bd} \\ K_{db} & K_{dd} \end{bmatrix} \begin{Bmatrix} \{y_b\} \\ \{y_d\} \end{Bmatrix} + \begin{bmatrix} [0] & [0] \\ C_{db} & C_{dd} \end{bmatrix} \begin{Bmatrix} \{\dot{y}_b\} \\ \{\dot{y}_d\} \end{Bmatrix} + \begin{bmatrix} [0] & [0] \\ M_{db} & M_{dd} \end{bmatrix} \begin{Bmatrix} \{\ddot{y}_b\} \\ \{\ddot{y}_d\} \end{Bmatrix} = 0 \tag{36}$$

The general solution of the system of equations 36 is considered in the following harmonic form

© 2023 IAU, Arak Branch

$$\{y\} = \{\vec{y}\}\exp(\omega t) \tag{37}$$

Substituting Eq. (37) into Eq. (36), yields

$$\left(\omega^2[M] + \omega[C] + [K]\right)\{\bar{y}_d\} = \{0\} \tag{38}$$

To have non definite solution, one should solve the following equation

$$\det\left(\omega^2[M] + \omega[C] + [K]\right) = 0 \tag{39}$$

By solving Eq. (39), the eigenvalues and eigenvectors will be obtained.

7 BOUNDARY CONDITIONS

Boundary conditions of clamped end of shell is considered as:

$$u = 0, v = 0, w = 0, \frac{\partial w}{\partial x} = 0 \tag{40a}$$

On the other hand, boundary conditions of simple end is

$$u = 0, v = 0, w = 0, \frac{\partial^2 w}{\partial x^2} = 0 \tag{40b}$$

Using differential quadrature method, boundary conditions for clamped- clamped tube is defined as:

$$U(0) = V(0) = W(0) = 0 \tag{41a}$$

$$\sum_{j=1}^{N} A_{1j}^{(1)} W_j = 0 \tag{41b}$$

$$U(L) = V(L) = W(L) = 0 \tag{41c}$$

$$\sum_{j=1}^{N} A_{Nj}^{(1)} W_j = 0 \tag{41d}$$

Boundary conditions for simple- simple tube is defined as:

$$U(0) = V(0) = W(0) = 0 \tag{42a}$$

$$\sum_{j=1}^{N} A_{1j}^{(2)} W_j = 0 \tag{42b}$$

$$U(L) = V(L) = W(L) = 0 \tag{42c}$$

© 2023 IAU, Arak Branch

$$\sum_{j=1}^{N} A_{1j}^{(2)} W_j = 0 \tag{42d}$$

Boundary conditions for clamped- simple tube is defined as:

$$U(0) = V(0) = W(0) = 0 \tag{43a}$$

$$\sum_{j=1}^{N} A_{1j}^{(1)} W_j = 0 \tag{43b}$$

$$U(L) = V(L) = W(L) = 0 \tag{43c}$$

$$\sum_{j=1}^{N} A_{1j}^{(2)} W_j = 0 \tag{43d}$$

8 VALIDATION

For validation purpose, the fundamental frequency results of cylindrical shell with $E_{11}/E_{22} = 40$, $\nu_{12} = 0.25$ and $G_{12}/E_{22} = 0.5$ for [45/-45] layer orientation, clamped-clamped ends, and different length and thickness ratios are compared with the results of shu [15], in table 1. It is seen that the deviations of results with those given in this paper are not significant.

Table 1
Natural dimensionless frequency of clamped- clamped shell.

		L/R=1	*L/R*=2	*L/R*=5	*L/R*=10	*L/R*=20
h/R=0.01	Present	0.6925	0.3984	0.2035	0.1138	0.0591
	Shu	0.6867	0.3493	0.2028	0.1131	0.0590
h/R =0.02	Present	0.9520	0.5111	0.2484	0.1395	0.0766
	Shu	0.9378	0.5020	0.2440	0.1385	0.0754
h/R =0.03	Present	1.1698	0.5951	0.2910	0.1539	0.0992
	Shu	1.1469	0.5811	0.2842	0.1510	0.0968
h/R =0.04	Present	1.3932	0.6578	0.3039	0.1720	0.1008
	Shu	1.3582	0.6377	0.2945	0.1670	0.1003
h/R =0.05	Present	1.6016	0.7289	0.3193	0.1928	0.1011
	Shu	1.5579	0.7014	0.3071	0.1855	0.1001

The dimensionless frequency and flow velocity are defined as follows:

$$\Omega = 2\pi R\,\omega\sqrt{\frac{\rho h}{A_{11}}} \qquad V = Lu\sqrt{\frac{\rho A}{D_{11}}}$$

9 RESULTS AND DISCUSSION

Hereafter, imaginary part of the eigenvalues denotes the natural frequency and the real part designates oscillation frequency of the roots of eigen-Eq. (39). In Fig. 3, Real and Imaginary parts of calculated eigenvalues for a four

© 2023 IAU, Arak Branch

layer composite tube with layer properties and dimensions given in Table 2, and stacking sequence [0/90]*s* conveying fluid flow, with two boundary conditions (clamped and simple ends) are compared.

Table 2
Material properties and dimensions of tube, Type 1.

E_1 =200 *GPa*	E_1 =20 *GPa*	υ_{12} =0.25	G_{12} =6 *GPa*	L=2 *m*	R=0.1 *m*	ρ=2000 kg/m^3

The natural frequencies are represented by imaginary parts of the first mode eigenvalues. It is seen that for low flow velocities, the real part is zero, however, by increasing the flow velocity, at V=3.1 and 6.2 (respectively for simple and clamped ends) the real part emerges, starting the pitchfork bifurcation instability and the imaginary parts of roots of eigen-equation become negative, indicating the forces exerted by flow and acceleration are not balanced by internal/ structural damping of system. Also, both the dimensionless critical flow velocity and oscillation frequencies are larger for tube with clamped boundary conditions.

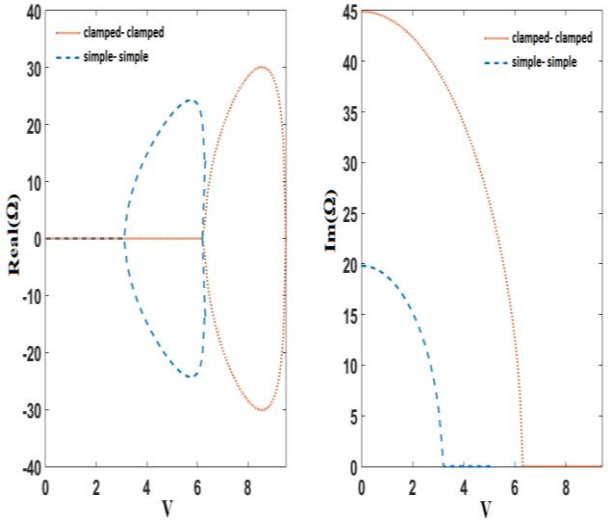

Fig.3
Comparing Root locus for two boundary conditions.

In Fig. 4, the vibration mode effect is studied. The calculated frequencies of composite tube with simple-simple boundary conditions and [0/90]*s* layer orientation is plotted for three lowest modes and different dimensionless flow velocities up to 10 . According to real part, the roots become linearly unstable as soon as one of the displacement modes has a positive growth rate ($Re > 0$). This happens at faster flow speed for higher modes. The imaginary parts of higher modes show different behavior from the fundamental mode in terms of frequency. On the whole, the equilibrium position of tube loses stability by flutter at V= 3.1, 6.2 and 9.5, for the three lowest modes, respectively.

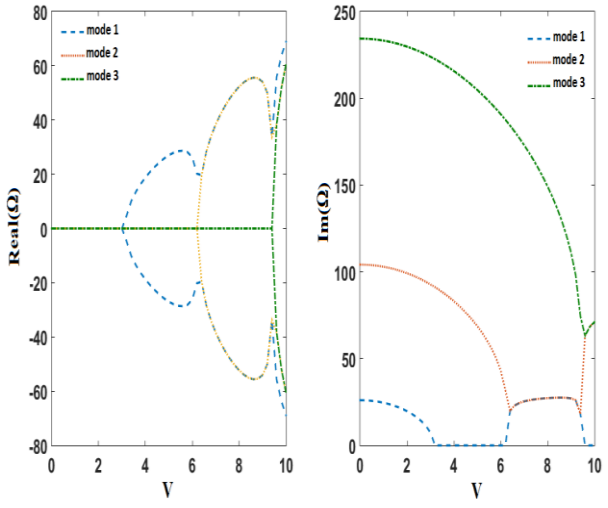

Fig.4
Comparing the effects of three lowest modes.

© 2023 IAU, Arak Branch

In Fig. 5, the effect of number of layers on frequency and attenuation of the response are studied for composite tube with [0/90]*s* and [45/-45]*s* patterns of lamination and simple- simple boundary conditions. It is expected that increasing the number of layers, causes an escalation in bending stiffness and therefore natural frequency, but has no effect on dimensionless critical flow velocity.

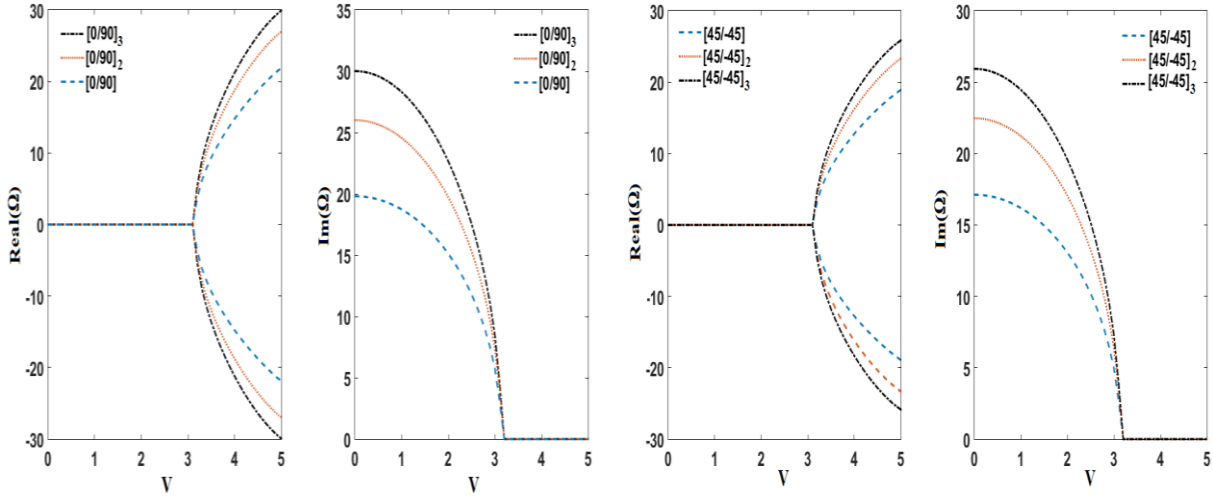

Fig.5
Effect of number of layers.

In Fig. 6, fundamental frequencies of composite tube with simple- simple boundary conditions for different fiber orientations are shown. It is seen that fiber angle has no effect on dimensionless critical velocity of fluid, but it could change the values of natural frequencies. The cross-ply causes higher stiffness than the other two angle ply.

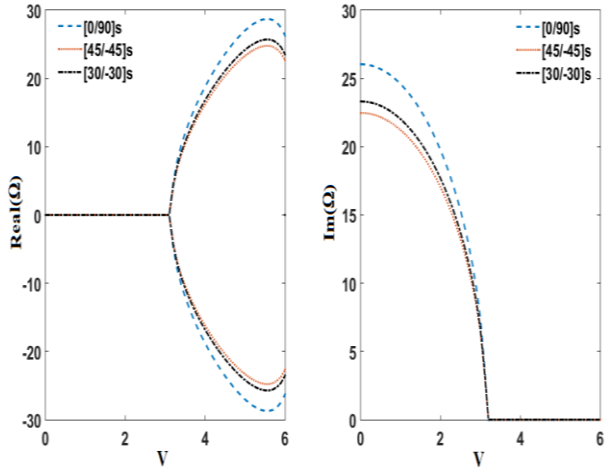

Fig.6
Effect of angle of fibers.

In Fig. 7, eigenvalue variations of the previously used composite tube with simple- simple ends, and layer orientation of [0/90]*s* are compared with those of a more flexible composite material type given in Table 3. It is obvious that type of composite has no effect on dimensionless critical velocity but has significant effects on oscillations frequency.

Table 3
Material properties and dimensions of tube, Type 2.

E_1 =145 *GPa*	E_1 =10 *GPa*	υ_{12} =0.3	G_{12} =4 *GPa*	L=2 *m*	R=0.1 *m*	ρ=2000 kg/m^3

© 2023 IAU, Arak Branch

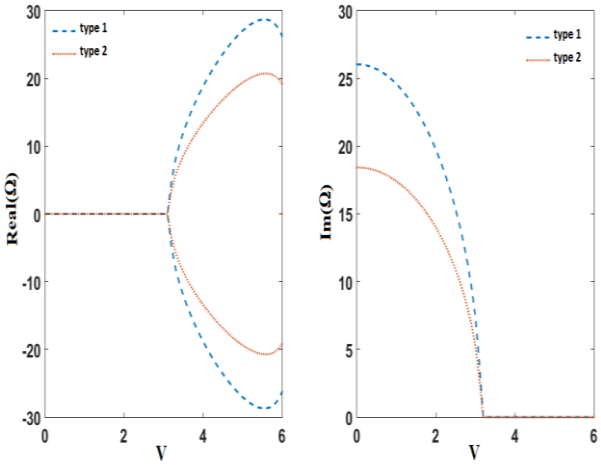

Fig.7
Effect of types of composite.

In Fig. 8, the effects of fluid density is illustrated for composite tube type 1 with simple- simple boundary conditions, and [0/90]*s* layer orientation. It is seen that density of fluid has no effect on dimensionless critical velocity of fluid, but has sufficient effect on dynamic behavior of system. Increasing density of fluid causes decline in vibration frequency at higher velocities, while this takes place for natural frequency when fluid moves slower.

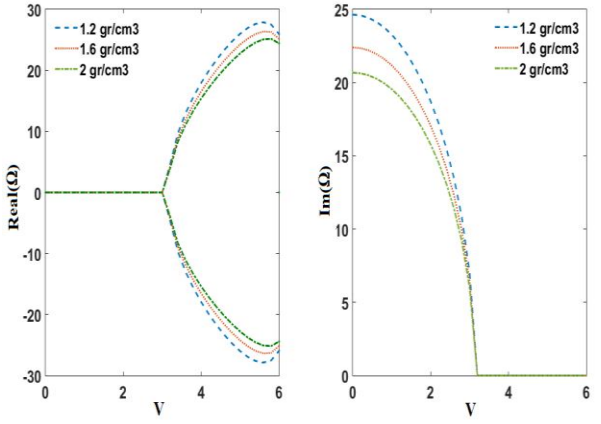

Fig.8
Effect of fluid density.

In Fig. 9, effect of temperature gradient between pipe and environment on frequency of composite tube type 1, with layer orientation of [0/90]*s*, and simple- simple boundary conditions is shown. By increasing temperature of pipe, dimensionless critical flow velocity reduces, on the other hand, thermal stress acts as compression force on shell, resulting a change in stiffness of tube and lower natural frequency for warmer tube.

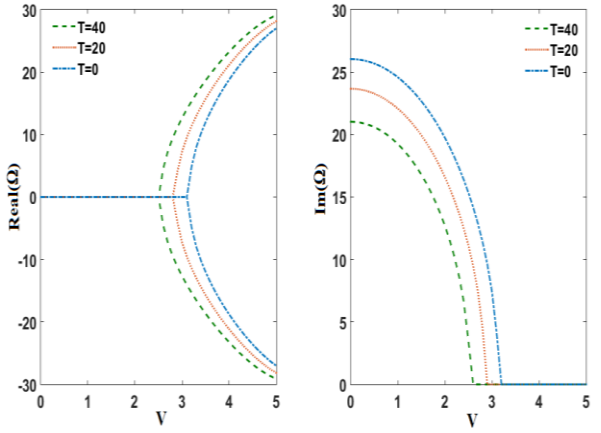

Fig.9
Effects of temperature tension.

© 2023 IAU, Arak Branch

In Fig. 10, the effect of applied voltage to ring piezoelectric actuator is studied. Tube is considered as composite type 1 with stacking [0/90]*s*, and simple- simple boundary conditions. Piezoelectric ring actuator is placed at the middle of tube. The length of ring is taken one quarter the tube length. The piezoelectric material is considered isotropic PZT-5H with the material properties given in Table 4.

Table 4
Material properties of PZT-5H.

E_1 GPa	61
E_2 GPa	61
υ_{12}	0.31
d_{31} C/m^2	274×10^{-12}
d_{32} C/m^2	235×10^{-12}
ρ Kg/m^3	7200

The maximum applied voltage in radial direction is 200 *mV*, below the actuation saturation limit. It is shown that applying voltage to ring piezoelectric actuator induces bending stiffness in the shell and therefore gives rise to divergence or flutter-type instability and natural frequency of system is increased.

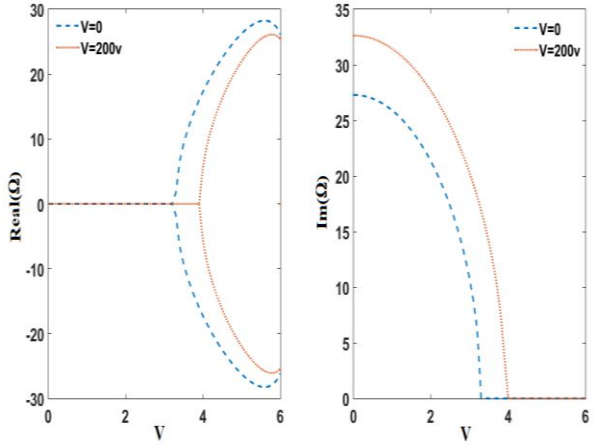

Fig.10
Effect of applying voltage to ring piezoelectric actuator.

In Fig. 11, effects of piezoelectric ring actuator length is studied for three length ratios (*a*/*L*). The ring is attached on the middle of the tube and a 200 *mV* voltage is applied to it. As it is expected, by increasing the length of piezo-ring, dimensionless critical flow velocity and natural frequency tend to increase proportionally.

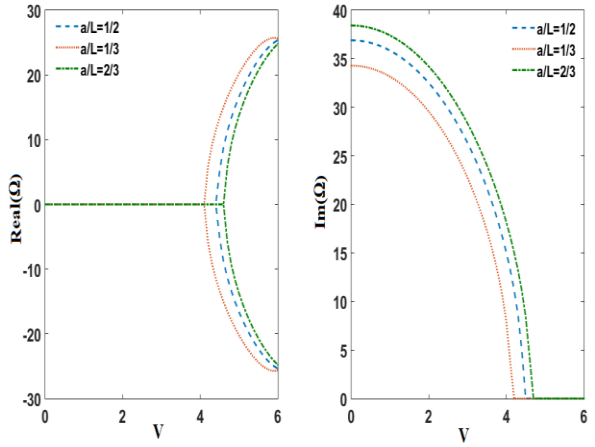

Fig.11
Effect of length of piezoelectric ring actuator.

© 2023 IAU, Arak Branch

10 CONCLUSIONS

An electro-thermo-mechanical theoretical analysis for vibration of composite tube conveying fluid equipped with piezoelectric ring is developed. The following conclusions are obtained in this study:

- Dimensionless critical flow velocity in clamped- clamped pipes is greater than simple- simple supported pipes with the same properties.
- Regarding fluid flow effects, it has been shown that the fluid flow rate is basically an effective factor on decreasing natural frequency leading to flutter of the tube.
- Increasing density of fluid causes decrease in natural and oscillatory frequencies, but it has no effect on dimensionless critical velocity.
- Critical flow velocity in pipes with higher temperature is lower, as well as their natural frequency.
- It is inferred that stability of the system is strongly dependent on the electric field so that increasing the imposed positive electric potential to piezoelectric ring significantly increases the stability of the system.
- Applying the electro-thermal field is the most effective parameter in avoiding the dynamic instability of the composite fluid carrying pipe.

REFERENCES

[1] Faria A.R., Almeida S.F.M., 1998, Axisymmetric actuation of composite cylindrical thin shells with piezoelectric rings, *Smart Material Structures* **7**: 843-850.

[2] Zhang Y.L., Gorman D.G., Reese J. M., 2003, Vibration of prestressed thin cylindrical shells conveying fluid, *Thin-Walled Structures* **41**: 1103-1127.

[3] Civalek O., 2004, Application of differential quadrature (DQ) and harmonic differential quadrature (HDQ) for buckling analysis of thin isotropic plates and elastic columns, *Engineering Structures* **26**: 171-186.

[4] Reddy J.N., Wang C.M., 2004, *Dynamics of Fluid Conveying Beams*, Centre for Offshore Research and Engineering National University of Singapore.

[5] Saviz M.R., Shakeri M., Yas M.H., 2009, Layer wise finite element analysis of laminated cylindrical shell with piezoelectric rings under dynamic load, *Mechanics of Advanced Materials and Structures* **16**: 20-32.

[6] Karagiozis K., Amabili M., Paidoussis M.P., 2010, Nonlinear dynamics of harmonically excited circular cylindrical shells containing fluid flow, *Journal of Sound and Vibration* **329**: 3813-3834.

[7] Bochkarev S.A., Matveenko V.P., 2011, Natural Vibrations and instability of shells of revolution interacting with an internal fluid flow, *Journal of Sound and Vibration* **330**: 3084-3101.

[8] Jannesari H., Emami M.D., Karimpour H., 2012, Investigating the effect of viscosity and nonlocal effects on the stability of SWCNT conveying flowing fluid using nonlinear shell model, *Physics Letters A* **376**: 1137-1145.

[9] Ke L.L., Wang Y.S., Reddy J.N., 2014, Thermo-electro-mechanical vibration of size-dependendt piezoelectric cylindrical nanoshells under various boundary conditions, *Composite Structures* **116**: 626-636.

[10] Maalawi K.Y., Abouel-fotouh A.M., EI Bayoumi M., Yehia Khaled Ahmad Ali, 2016, Design of composite pipes conveying fluid of improved stability characteristics, *International Journal of Applied Engineering Research* **11**: 7633-7639.

[11] KhodamiMaraghi Z., GhorbanpourArani A., Kolahchi R., Amir S., Bagheri M.R., 2013, Nonlocal vibration and instability of embedded DWBNNT conveying viscose fluid, *Composites: Part B* **45**: 423-432.

[12] Raminnia M., Biglari H., VakiliTahami F., 2016, Nonlinear higher order Reddy theory for temperature dependent vibration and instability of embedded functionally graded pipes conveying fluid-nanoparticle mixture, *Structural Engineering and Mechanics* **59**: 153-186.

[13] Reddy J.N., 2004, *Mechanics of laminated composite plates and shells, Theory and analysis*, CRC Press.

[14] GhorbanpourArani A., Kolahchi R., KhoddamiMaraghi Z., 2013, Nonlinear vibration and instability of embedded double-walled boron nitride nanotubes based on nonlocal cylindrical shell theory, *Applied Mathematical Modelling* **37**: 7685-7707.

[15] Shu C., Du H., 1997, Free vibration analysis of laminated composite cylindrical shell by DQM, *Composite Technology Part B* **28**: 267-274.

© 2023 IAU, Arak Branch